

Spatial extent of an outbreak in animal epidemics

Eric Dumonteil *, Satya N. Majumdar †, Alberto Rosso †, and Andrea Zoia *,

*CEA/Saclay, DEN/DM2S/SERMA/LTSD, 91191 Gif-sur-Yvette Cedex, France, and †CNRS - Université Paris-Sud, LPTMS, UMR8626, 91405 Orsay Cedex, France

Submitted to Proceedings of the National Academy of Sciences of the United States of America

Characterizing the spatial extent of epidemics at the outbreak stage is key to controlling the evolution of the disease. At the outbreak, the number of infected individuals is typically small, so that fluctuations around their average are important: then, it is commonly assumed that the susceptible-infected-recovered (SIR) mechanism can be described by a stochastic birth-death process of Galton-Watson type. The displacements of the infected individuals can be modelled by resorting to Brownian motion, which is applicable when long-range movements and complex network interactions can be safely neglected, as in case of animal epidemics. In this context, the spatial extent of an epidemic can be assessed by computing the convex hull enclosing the infected individuals at a given time. We derive the exact evolution equations for the mean perimeter and the mean area of the convex hull, and compare them with Monte Carlo simulations.

Epidemics | Branching Brownian motion | Convex hull

Models of epidemics traditionally consider three classes of populations, namely, the susceptibles (S), the infected (I), and the recovered (R). This provides the basis of the so-called SIR model [1, 2], a *fully connected mean-field* model where the population sizes of the three species evolve with time t via the coupled nonlinear equations: $dS/dt = -\beta IS$; $dI/dt = \beta IS - \gamma I$ and $dR/dt = \gamma I$. Here γ is the rate at which an infected individual recovers and β denotes the rate at which it transmits the disease to a susceptible [4, 5, 6]. In the simplest version of these models, the recovered can not be infected again. These rate equations conserve the total population size $I(t) + S(t) + R(t) = N$, and one assumes that initially there is only one infected individual and the rest of the population is susceptible: $I(0) = 1$, $S(0) = N - 1$, and $R(0) = 0$. Of particular interest is the outbreak stage, i.e., the early times of the epidemic process, when the susceptible population is much larger than the number of infected or recovered. During this regime, for large N , the susceptible population hardly evolves and stays $S(t) \approx N$, so that nonlinear effects can be safely neglected and one can just monitor the evolution of the *infected population alone*: $dI/dt \approx (\beta N - \gamma)I(t)$. Thus, the ultimate fate of the epidemics depends on the key dimensionless parameter $R_0 = \beta N / \gamma$, which is called the reproduction rate. If $R_0 > 1$ the epidemic explodes and invades a finite fraction of the population, if $R_0 < 1$ the epidemic goes to extinction, and in the critical case $R_0 = 1$ the infected population remains constant [7, 8, 9].

This basic deterministic SIR has been generalized to a variety of both deterministic as well as stochastic models, whose distinct advantages and shortcomings are discussed at length in [3, 10, 11]. Generally speaking, stochastic models are more suitable in presence of a small number of infected individuals, when fluctuations around the average may be relevant [3, 10]. During the outbreak of epidemics, the infected population is typically small: in this regime, the evolution can be modeled by resorting to a stochastic birth-death branching process of the Galton-Watson type for the number of infected [3, 10, 11], where each infected individual transmits the disease to another individual at rate βN and recovers at rate γ . The epidemic may become endemic for $R_0 > 1$, becomes extinct for $R_0 < 1$, whereas for $R_0 = 1$ fluctuations are typically long lived and completely control the time evolution of the infected population [4, 5, 6].

How far in space can an epidemic spread? Branching processes alone are not sufficient to describe an outbreak, and spatial effects must necessarily be considered [1, 5, 12, 13, 14]. Quantifying the geographical spread of an epidemic is closely related to the modelling of the population displacements. Brownian motion is often considered as a paradigm for describing the migration of individuals, despite some well-known shortcomings: for instance, finite speed effects and preferential displacements are neglected. Most importantly, a number of recent studies have clearly shown that individuals geographically far apart can actually be closely related to each other through the so-called small-world connections, such as air traffic, public transportation and so on: then, the spread of epidemics among humans can not be realistically modelled without considering these complex networks of interconnections [15, 16, 17, 18]. Nonetheless, Brownian motion provides a reasonable basis for studying disease propagation in animals and possibly in plants (here, pathogen vectors are insects) [4].

While theoretical models based on branching Brownian motion have provided important insights on how the population size grows and fluctuates with time in a given domain [1, 5, 13, 14], another fundamental question is *how the spatial extension of the infected population evolves with time*. Assessing the geographical area travelled by a disease is key to the control of epidemics, and this is especially true at the outbreak, when confinement and vaccination could be most effective. One major challenge in this very practical field of disease control is how to quantify the area that needs to be quarantined during the outbreak. For animal epidemics, this issue has been investigated experimentally, for instance in the case of equine influenza [19]. The most popular and widely used method for this consists in recording the set of positions of the infected animals and, at each time instant, construct a *convex hull*, i.e., a *minimum convex polygon* surrounding the positions (Fig. 1; for a precise definition of the convex hull, see below). The convex hull at time t then provides a rough measure of the area over which the infections have spread up to time t . The convex hull method is also used to estimate the home range of animals, i.e., the territory explored by a herd of animals during their daily search for food [20, 21].

In this paper, we model the outbreak of an epidemic as a Galton-Watson branching process in presence of Brownian spatial diffusion. Despite infection dynamics being relatively simple, the corresponding convex hull is a rather complex function of the trajectories of the infected individuals up to time t , whose statistical properties seem to be a formidable problem. Our main goal is to characterize the time evolution

Reserved for Publication Footnotes

arXiv:1303.3868v2 [q-bio.PE] 18 Mar 2013

of the convex hull associated to this process, in particular its mean perimeter and area.

The rest of the paper is organized as follows. We first describe precisely the model and summarize our main results. Then, we provide a derivation of our analytical findings, supported by extensive numerical simulations. We conclude with perspectives and discussions. Some details of the computations are relegated to the Supplementary Material.

The model and the main results

Consider a population of N individuals, uniformly distributed in a two dimensional plane, with a single infected at the origin at the initial time. At the outbreak, it is sufficient to keep track of the positions of the infected, which will be marked as ‘particles’. The dynamics of the infected individuals is governed by the following stochastic rules. In a small time interval dt , each infected alternatively

(i) recovers with probability γdt . This corresponds to the death of a particle with rate γ .

(ii) infects, *via local contact*, a new susceptible individual from the background with probability $b dt$. This corresponds to the birth of a new particle that can subsequently diffuse. The originally infected particle still remains infected, which means that the trajectory of the originally infected particle branches into two new trajectories. The rate b replaces the rate βN in the SIR or the Galton-Watson process mentioned before.

(iii) diffuses with diffusion constant D with probability $1 - (\gamma + b) dt$. The coordinates $\{x(t), y(t)\}$ of the particle get updated to the new values $\{x(t) + \eta_x(t) dt, y(t) + \eta_y(t) dt\}$, where $\eta_x(t)$ and $\eta_y(t)$ are independent Gaussian white noises with zero mean and correlators $\langle \eta_x(t) \eta_x(t') \rangle = 2D\delta(t - t')$, $\langle \eta_y(t) \eta_y(t') \rangle = 2D\delta(t - t')$ and $\langle \eta_x(t) \eta_y(t') \rangle = 0$.

The only dimensionless parameter in the model is the ratio $R_0 = b/\gamma$, i.e. the basic reproduction number.

Consider now a particular history of the assembly of the trajectories of all the infected individuals up to time t , starting from a single infected initially at the origin (see Fig. 1). For every realization of the process, we construct the associated convex hull C . To visualize the convex hull, imagine stretching a rubber band so that it includes all the points of the set at time t inside it and then releasing the rubber band. It shrinks and finally gets stuck when it touches some points of the set, so that it can not shrink any further. This final shape is precisely the convex hull associated to this set.

In this paper, we show that the mean perimeter $\langle L(t) \rangle$ and the mean area $\langle A(t) \rangle$ of the convex hull are ruled by two coupled nonlinear partial differential equations that can be solved numerically for all t (see Fig. 2). The asymptotic behavior for large t can be determined analytically for the critical ($R_0 = 1$), subcritical ($R_0 < 1$) and supercritical ($R_0 > 1$) regimes. In particular, in the *critical* regime the mean perimeter *saturates* to a finite value as $t \rightarrow \infty$, while the mean area *diverges logarithmically* for large t

$$\langle L(t \rightarrow \infty) \rangle = 2\pi \sqrt{\frac{6D}{\gamma}} + \mathcal{O}(t^{-1/2}) \quad [1]$$

$$\langle A(t \rightarrow \infty) \rangle = \frac{24\pi D}{5\gamma} \ln t + \mathcal{O}(1). \quad [2]$$

This prediction seems rather paradoxical at a first glance. How can the perimeter of a polygon be finite while its area is divergent? The resolution to this paradox owes its origin precisely to statistical fluctuations. The results in Eqs. [1] and [2] are true only on average. Of course, for each sample, the convex hull has a finite perimeter and a finite area. How-

ever, as we later show, the probability distributions of these random variables have power-law tails at long time limits. For instance, while $\text{Prob}(L, t \rightarrow \infty) \sim L^{-3}$ for large L (thus leading to a finite first moment), the area distribution behaves as $\text{Prob}(A, t \rightarrow \infty) \sim A^{-2}$ for large A . Hence the mean area is divergent as $t \rightarrow \infty$ (see Fig. 2).

When $R_0 \neq 1$, the evolution of the epidemic is controlled by a characteristic time t^* , which scales like $t^* \sim |R_0 - 1|^{-1}$. For times $t < t^*$ the epidemic behaves as in the critical regime. In the *subcritical* regime, for $t > t^*$ the quantities $\langle L(t) \rangle$ and $\langle A(t) \rangle$ rapidly saturate and the epidemic goes eventually to extinction. In contrast, in the *supercritical* regime (which is the most relevant for virulent epidemics that spread fast), a new time-dependent behavior emerges when $t > t^*$, since there exists a finite probability (namely $1 - 1/R_0$) that epidemic never goes to extinction (Fig. 5). More precisely, we later show that

$$\langle L(t \gg t^*) \rangle = 4\pi \left(1 - \frac{1}{R_0}\right) \sqrt{D\gamma(R_0 - 1)} t \quad [3]$$

$$\langle A(t \gg t^*) \rangle = 4\pi \left(1 - \frac{1}{R_0}\right) D\gamma(R_0 - 1) t^2. \quad [4]$$

The ballistic growth of the convex hull stems from an underlying travelling front solution of the non-linear equation governing the convex hull behavior. Indeed, the prefactor of the perimeter growth is proportional to the front velocity $v^* = 2\sqrt{D\gamma(R_0 - 1)}$. As time increases, the susceptible population decreases due to the growth of the infected individuals: this depletion effect leads to a breakdown of the outbreak regime and to a slowing down of the epidemic propagation.

The statistics of the convex hull

Characterizing the fluctuating geometry of C is a formidable task even in absence of branching ($b = 0$) and death ($\gamma = 0$), i.e., purely for diffusion process in two dimensions. Major recent breakthroughs have nonetheless been obtained for diffusion processes [23, 24] by a clever adaptation of the Cauchy’s integral geometric formulae for the perimeter and area of any closed convex curve in two dimensions. In fact, the problem of computing the mean perimeter and area of the convex hull of *any generic two dimensional* stochastic process can be mapped, using Cauchy’s formulae, to the problem of computing the moments of the maximum and the time at which the maximum occurs for the associated one dimensional component stochastic process [23, 24]. This was used for computing, e.g., the mean perimeter and area of the convex hull of a two dimensional regular Brownian motion [23, 24] and of a two dimensional random acceleration process [25].

Our main idea here is to extend this method to compute the convex hull statistics for the two dimensional branching Brownian motion. Following this general mapping and using isotropy in space (see Supplementary Materials), the average perimeter and area of the convex hull are given by

$$\langle L(t) \rangle = 2\pi \langle x_m(t) \rangle \quad [5]$$

$$\langle A(t) \rangle = \pi [\langle x_m^2(t) \rangle - \langle y^2(t_m) \rangle], \quad [6]$$

where x_m is the maximum displacement of our two-dimensional stochastic process in the x direction up to time t , t_m is the time at which the maximum displacement along x direction occurs and $y(t_m)$ is the ordinate of the process at t_m , i.e., when the displacement along the x direction is maximal. A schematic representation is provided in Fig. 4, where the global maximum x_m is achieved by one single infected individual, whose path is marked in red. A crucial observation is that the y component of the trajectory connecting O to

this red path is a regular one dimensional Brownian motion. Hence, given t_m and t , clearly $\langle y^2(t_m) \rangle = 2D\langle t_m \rangle$. Therefore,

$$\langle A(t) \rangle = \pi [\langle x_m^2(t) \rangle - 2D\langle t_m(t) \rangle]. \quad [7]$$

Equations [5] and [7] thus show that the mean perimeter and area of the epidemics outbreak are related to the extreme statistics of a one dimensional branching Brownian motion with death. Indeed, if we can compute the joint distribution $P_t(x_m, t_m)$, we can in turn compute the three moments $\langle x_m \rangle$, $\langle x_m^2 \rangle$ and $\langle t_m \rangle$ that are needed in Eqs. [5] and [7]. We show below that this can be performed exactly.

The convex hull perimeter and the maximum x_m . For the average perimeter, we just need the first moment $\langle x_m(t) \rangle = \int_0^\infty x_m q_t(x_m) dx_m$, where $q_t(x_m)$ denotes the probability density of the of the maximum of the one dimensional component process. It is convenient to consider the cumulative distribution $Q_t(x_m)$ i.e., the probability that the maximum x -displacement stays below a given value x_m up to time t . Then, $q_t(x_m) = dQ_t(x_m)/dx_m$ and $\langle x_m(t) \rangle = \int_0^\infty [1 - Q_t(x_m)] dx_m$. Since the process starts at the origin, its maximum x -displacement, for any time t , is necessarily nonnegative, i.e., $x_m \geq 0$. We next write down a backward Fokker-Planck equation describing the evolution of $Q_t(x_m)$ by considering the three mutually exclusive stochastic moves in a small time interval dt : starting at the origin at $t = 0$, the walker during the subsequent interval $[0, dt]$ dies with probability γdt , infects another individual (i.e., branches) with probability $b dt = R_0 \gamma dt$, or diffuses by a random displacement $\Delta x = \eta_x(0) dt$ with probability $1 - \gamma(1 + R_0)dt$. In the last case, its new starting position is Δx for the subsequent evolution. Hence, for all $x_m \geq 0$, one can write

$$Q_{t+dt}(x_m) = \gamma dt + R_0 \gamma dt Q_t^2(x_m) + [1 - \gamma(R_0 + 1)] dt \langle Q_t(x_m - \Delta x) \rangle, \quad [8]$$

where the expectation $\langle \rangle$ is taken with respect to the random displacements Δx . The first term means that if the process dies right at the start, its maximum up to t is clearly 0 and hence is necessarily less than x_m . The second term denotes the fact that in case of branching the maximum of each branch stays below x_m : since the branches are independent, one gets a square. The third term corresponds to diffusion. By using $\langle \Delta x \rangle = 0$ and $\langle \Delta x^2 \rangle = 2Ddt$ and expanding Eq. [8] to the first order in dt and second order in Δx we obtain

$$\frac{\partial}{\partial t} Q = D \frac{\partial^2}{\partial x_m^2} Q - \gamma(R_0 + 1)Q + \gamma R_0 Q^2 + \gamma \quad [9]$$

for $x_m \geq 0$, satisfying the boundary conditions $Q_t(0) = 0$ and $Q_t(\infty) = 1$, and the initial condition $Q_0(x_m) = \Theta(x_m)$, where Θ is the Heaviside step function. Hence from Eq. [5]

$$\langle L(t) \rangle = 2\pi \int_0^\infty [1 - Q_t(x_m)] dx_m. \quad [10]$$

Equation [9] can be solved numerically for all t and all R_0 , which allows subsequently computing $\langle L(t) \rangle$ in Eq. [10] (details and figures are provided in the Supplementary Material).

The convex hull area. To compute the average area in Eq. [7], we need to evaluate $\langle x_m^2(t) \rangle$ as well as $\langle t_m \rangle$. Once the cumulative distribution $Q_t(x_m)$ is known, the second moment $\langle x_m^2(t) \rangle$ can be directly computed by integration, namely, $\langle x_m^2(t) \rangle = \int_0^\infty dx_m 2x_m(1 - Q_t(x_m))$. To determine $\langle t_m \rangle$, we need to also compute the probability density $p_t(t_m)$ of the random variable t_m . Unfortunately, writing down a closed equation for

$p_t(t_m)$ is hardly feasible. Instead, we first define $P_t(x_m, t_m)$ as the joint probability density that the maximum of the x component achieves the value x_m at time t_m , when the full process is observed up to time t . Then, we derive a backward evolution equation for $P_t(x_m, t_m)$ and then integrate out x_m to derive the marginal density $p_t(t_m) = \int_0^\infty P_t(x_m, t_m) dx_m$. Following the same arguments as those used for $Q_t(x_m)$ yields a backward equation for $P_t(x_m, t_m)$:

$$P_{t+dt}(x_m, t_m) = [1 - \gamma(R_0 + 1)dt] \langle P_t(x_m - \Delta x, t_m - dt) \rangle + 2\gamma R_0 dt Q_t(x_m) P_t(x_m, t_m - dt). \quad [11]$$

The first term at the right hand side represents the contribution from diffusion. The second term represents the contribution from branching: we require that one of them attains the maximum x_m at the time $t_m - dt$, whereas the other stays below x_m ($Q_t(x_m)$ being the probability that this condition is satisfied). The factor 2 comes from the interchangeability of the particles. Developing Eq. [11] to leading order gives

$$\left[\frac{\partial}{\partial t} + \frac{\partial}{\partial t_m} \right] P_t = \left[D \frac{\partial^2}{\partial x_m^2} - \gamma(R_0 + 1) + 2\gamma R_0 Q_t \right] P_t. \quad [12]$$

This equation describes the time evolution of $P_t(x_m, t_m)$ in the region $x_m \geq 0$ and $0 \leq t_m \leq t$. It starts from the initial condition $P_0(x_m, t_m) = \delta(x_m)\delta(t_m)$ (since the process begins with a single infected with x component located at $x = 0$, it implies that at $t = 0$ the maximum $x_m = 0$ and also $t_m = 0$). For any $t > 0$ and $x_m > 0$, we have the condition $P_t(x_m, 0) = 0$. We need to also specify the boundary conditions at $x_m = 0$ and $x_m \rightarrow \infty$, which read (i) $P_t(\infty, t_m) = 0$ (since for finite t the maximum is necessarily finite) and (ii) $P_t(0, t_m) = \delta(t_m) q_t(x_m)|_{x_m=0}$. The latter condition comes from the fact that, if $x_m = 0$, this corresponds to the event that the x component of the entire process, starting at 0 initially, stays below 0 in the time interval $[0, t]$, which happens with probability $q_t(x_m)|_{x_m=0}$: consequently, t_m must necessarily be 0. Furthermore, by integrating $P_t(x_m, t_m)$ with respect to t_m we recover the marginal density $q_t(x_m)$.

The numerical integration of the full Eq. [12] would be rather cumbersome. Fortunately, we do not need this. Since we are only interested in $\langle t_m \rangle$, it is convenient to introduce

$$T_t(x_m) = \int_0^t t_m P_t(x_m, t_m) dt_m, \quad [13]$$

from which the average follows as $\langle t_m \rangle = \int dx_m T_t(x_m)$. Multiplying Eq. [12] by t_m and integrating by parts we get

$$\frac{\partial}{\partial t} T_t - q_t(x_m) = \left[D \frac{\partial^2}{\partial x_m^2} + 2\gamma R_0 Q_t - \gamma(R_0 + 1) \right] T_t, \quad [14]$$

with the initial condition $T_0(x_m) = 0$, and the boundary conditions $T_t(0) = 0$ and $T_t(\infty) = 0$. Eq. [14] can be integrated numerically, together with Eq. [9] (details are provided in the Supplementary Material), and the behavior of

$$\langle A(t) \rangle = \pi \int_0^\infty dx_m [2x_m(1 - Q_t(x_m)) - T_t(x_m)] \quad [15]$$

as a function of time is illustrated in Fig. 2.

The critical regime. We now focus on the critical regime $R_0 = 1$. We begin with the average perimeter: for $R_0 = 1$, Eq. [9] admits a stationary solution as $t \rightarrow \infty$, which can be obtained by setting $\partial Q/\partial t = 0$ and solving the resulting differential equation. In fact, this stationary solution was already known in the context of the genetic propagation of a mutant allele [22]. Taking the derivative of this solution with

respect to x_m , we get the stationary probability density of the maximum x_m

$$q_\infty(x_m) = \partial_{x_m} Q_\infty(x_m) = \frac{2\sqrt{\frac{\gamma}{6D}}}{\left(1 + \sqrt{\frac{\gamma}{6D}}x_m\right)^3}. \quad [16]$$

The average is $\langle x_m \rangle = \int_0^\infty x_m q_\infty(x_m) dx_m = \sqrt{6D/\gamma}$, which yields then Eq. [1] for the average perimeter of the convex hull at late times.

To compute the average area in Eq. [7], we need to also evaluate the second moment $\langle x_m^2(t) \rangle$, which diverges as $t \rightarrow \infty$, due to the power-law tail of the stationary probability density $q_\infty(x_m) \propto x_m^{-3}$ for large x_m . Hence, we need to consider large but finite t . In this case, the time dependent probability density $q_t(x_m)$ displays a scaling form which can be conveniently written as

$$q_t(x_m) \simeq q_\infty(x_m) f\left(\frac{x_m}{\sqrt{Dt}}\right), \quad [17]$$

where $f(z)$ is a rapidly decaying function with $f(z \ll 1) \simeq 1$, and $f(z \gg 1) \simeq 0$. Using the scaling form of Eq. [17] and Eq. [9] one can derive a differential equation for $f(z)$. But it turns out that we do not really need the solution of $f(z)$.

From Eq. [17] we see that the asymptotic power-law decay of $q_t(x_m)$ for large x_m has a cut-off around $x_m^* \sim \sqrt{Dt}$ and $f(z)$ is the cut-off function. The second moment at finite but large times t is given by $\langle x_m^2(t) \rangle = \int_0^\infty x_m^2 q_t(x_m) dx_m$. Substituting the scaling form and cutting off the integral over x_m at $x_m^* = c\sqrt{t}$ (where the constant c depends on the precise form of $f(z)$) we get, to leading order for large t ,

$$\langle x_m^2(t) \rangle \simeq \int_0^{x_m^*} x_m^2 q_\infty(x_m) dx_m \simeq \frac{6D}{\gamma} \ln t. \quad [18]$$

Thus, interestingly the leading order result is universal, i.e. independent of the details of the cut-off function $f(z)$ (the c -dependence is only in the subleading term). To complete the characterization of $\langle A(t) \rangle$ in Eq. [7], we still need to determine $\langle t_m \rangle$: in the Supplementary Material we explicitly determine the stationary solution $P_\infty(x_m, t_m)$ for $R_0 = 1$. By following the same arguments as for $\langle x_m^2(t) \rangle$, we show that

$$\langle t_m \rangle \simeq \frac{3}{5\gamma} \ln t \quad [19]$$

for large t , which leads again to a logarithmic divergence in time. Finally, substituting Eqs. [18] and [19] in Eq. [7] gives the result announced in Eq. [2].

A deeper understanding of the statistical properties of the process would demand knowing the full distribution $\text{Prob}(L, t)$ and $\text{Prob}(A, t)$ of the perimeter and area. These seem rather hard to compute, but one can obtain the asymptotic tails of the distributions by resorting to scaling arguments. Following the lines of Cauchy's formula (see the Supplementary Material), it is reasonable to assume that for each sample the perimeter scales as $L(t) \sim x_m(t)$. We have seen that the distribution of $x_m(t)$ has a power-law tail for large t : $q_\infty(x_m) \sim x_m^{-3}$ for large x_m . Then, assuming the scaling $L(t) \sim x_m(t)$ and using $\text{Prob}(L, t \rightarrow \infty) dL \sim q_\infty(x_m) dx_m$, it follows that at late times the perimeter distribution also has a power-law tail: $\text{Prob}(L, t \rightarrow \infty) \sim L^{-3}$ for large L . Similarly, using the Cauchy formula for the area, we can reasonably assume that for each sample $A(t) \sim x_m^2(t)$ in the scaling regime. Once again, using $\text{Prob}(A, t \rightarrow \infty) dA = q_\infty(x_m) dx_m$, we find that the area distribution also converges, for large t , to a stationary distribution with a power-law tail: $\text{Prob}(A, t \rightarrow \infty) \sim A^{-2}$ for

large A . Moreover, the logarithmic divergence of the mean area calls for a precise ansatz on the tail of the area distribution, namely,

$$\text{Prob}(A, t) \xrightarrow{A \gg 1} \frac{24\pi D}{5\gamma} A^{-2} h\left(\frac{A}{Dt}\right), \quad [20]$$

where the scaling function $h(z)$ satisfies the conditions $h(z \ll 1) = 1$, and $h(z \gg 1) \simeq 0$. It is not difficult to verify that this is the only scaling compatible with Eq. [2]. These two results are consistent with the fact that for each sample typically $A(t) \sim L^2(t)$ at late times in the scaling regime. Our scaling predictions are in agreement with our Monte Carlo simulations (see Fig. 2). The power-law behavior of $\text{Prob}(A, t)$ implies that the average area is not representative of the typical behavior of the epidemic area, which is actually dominated by fluctuations and rare events, with likelihood given by Eq. [20].

The supercritical regime. When $R_0 > 1$, it is convenient to rewrite Eq. [9] in terms of $W(x_m, t) = 1 - Q(x_m, t)$:

$$\frac{\partial}{\partial t} W = D \frac{\partial^2}{\partial x_m^2} W + \gamma(R_0 - 1)W - \gamma R_0 W^2 \quad [21]$$

starting from the initial condition $W(x_m, 0) = 0$ for all $x_m > 0$ (see Fig. 5). From Eq. [10], $\langle L(t) \rangle = 2\pi \int_0^\infty W(x_m, t) dx_m$ is just the area under the curve $W(x_m, t)$ vs. x_m , up to a factor 2π . As $t \rightarrow \infty$, the system approaches a stationary state for all $R_0 \geq 1$, which can be obtained by setting $\partial_t W = 0$ in Eq. [21]. For $R_0 > 1$ the stationary solution $W(x_m, \infty)$ approaches the constant $1 - 1/R_0$ exponentially fast as $x_m \rightarrow \infty$, namely, $W(x_m, \infty) - 1 + R_0^{-1} \rightarrow \exp[-x_m/\xi]$, with a characteristic length scale $\xi = \sqrt{D/\gamma(R_0 - 1)}$. However, for finite but large t , $W(x_m, t)$ as a function of x_m has a two-step form: it first decreases from 1 to its asymptotic stationary value $1 - 1/R_0$ over the length scale ξ , and then decreases rather sharply from $1 - 1/R_0$ to 0. The frontier between the stationary asymptotic value $1 - 1/R_0$ (stable) and 0 (unstable) moves forward with time at constant velocity, thus creating a travelling front at the right end, which separates the stationary value $1 - 1/R_0$ to the left of the front and 0 to the right. This front advances with a constant velocity v^* that can be estimated using the standard velocity selection principle [27, 28, 29]. Near the front where the nonlinear term is negligible, the equation admits a travelling front solution: $W(x_m, t) \sim \exp[-\lambda(x_m - vt)]$, with a one parameter family of possible velocities $v(\lambda) = D\lambda + \gamma(R_0 - 1)/\lambda$, parametrized by λ . This dispersion relation $v(\lambda)$ has a minimum at $\lambda = \lambda^* = \sqrt{\gamma(R_0 - 1)/D}$, where $v^* = v(\lambda^*) = 2\sqrt{D\gamma(R_0 - 1)}$. According to the standard velocity selection principle [27, 28, 29], for a sufficiently sharp initial condition the system will choose this minimum velocity v^* . The width of the front remains of $\sim \mathcal{O}(1)$ at large t . Thus, due to this sharpness of the front, to leading order for large t one can approximate $W(x_m, t) \simeq (1 - 1/R_0)\Theta(v^*t - x_m)$ near the front. Hence, to leading order for large t one gets $\langle x_m(t) \rangle \simeq (1 - 1/R_0)v^*t$ and $\langle x_m^2(t) \rangle \simeq (1 - 1/R_0)(v^*t)^2$. The former gives, from Eq. [5], the result announced in Eq. [3]. For the mean area in Eq. [7], the term $\langle x_m^2(t) \rangle \sim t^2$ for large t dominates over $\langle t_m \rangle \sim t$ (which can be neglected), and we get the result announced in Eq. [3].

Conclusions

In this paper, we have developed a general procedure for assessing the time evolution of the convex hull associated to the outbreak of an epidemic. We find it extremely appealing that one can successfully use mathematical formulae (Cauchy's)

from two dimensional integral geometry to describe the spatial extent of an epidemic outbreak in relatively realistic situations. Admittedly, there are many assumptions in this epidemic model that are not quite realistic. For instance, we have ignored the fluctuations of the susceptible populations during the early stages of the epidemic: this hypothesis clearly breaks down at later times, when depletion effects begin to appear, due to the epidemic invading a thermodynamical fraction of the total population. In addition, we have assumed that the susceptibles are homogeneously distributed in space, which is not the case in reality. Nonetheless, it must be noticed that in practical applications whenever strong heterogeneities appear, such as mountains, deserts or oceans, one can split the analysis of the evolving phenomena by conveniently resorting to several distinct convex hulls, one for each separate region. For analogous reasons, the convex hull approach would not be suitable to characterize birth-death processes with long range displacements, such as for instance branching Lévy flights.

The model discussed in this paper based on branching Brownian motion is amenable to exact results. More generally, realistic models could be taken into account by resorting to cumbersome Monte Carlo simulations. The approach proposed in this paper paves the way for assessing the spatial dynamics of the epidemic by more conveniently solving two coupled nonlinear equations, under the assumption that the underlying process be rotationally invariant.

We conclude with an additional remark. In our computations of the mean perimeter and area, we have averaged over all realizations of the epidemics up to time t , including those which are already extinct at time t . It would also be interesting to consider averages only over the ensemble of epidemics that are still active at time t . In this case we expect different scaling laws for the mean perimeter and the mean area of the convex hull. In particular, in the critical case, we believe that the behavior would be much closer to that of a regular Brownian motion.

Appendix: Supplementary Materials

Cauchy's formula. The problem of determining the perimeter and the area of the convex hull of any two dimensional stochastic process $[x(\tau), y(\tau)]$ with $0 \leq \tau \leq t$ can be mapped to that of computing the statistics of the maximum and the time of occurrence of the maximum of the one dimensional component process $x(\tau)$ [23, 24]. This is achieved by resorting to a formula due to Cauchy, which applies to any closed convex curve C .

A sketch of the method is illustrated in Fig. 5. Choose the coordinates system such that the origin is inside the curve C and take a given direction θ . For fixed θ , consider a stick perpendicular to this direction and imagine bringing the stick from infinity and stop upon first touching the curve C . At this point, the distance $M(\theta)$ of the stick from the origin is called the support function in the direction θ . Intuitively, the support function measures how close can one get to the curve C in the direction θ , coming from infinity. Once the support function $M(\theta)$ is known, then Cauchy's formulas [30] give the perimeter L and the area A enclosed by C , namely

$$\begin{aligned} L &= \int_0^{2\pi} M(\theta) d\theta \\ A &= \frac{1}{2} \int_0^{2\pi} [M^2(\theta) - (M'(\theta))^2] d\theta, \end{aligned} \quad [22]$$

where $M'(\theta) = dM/d\theta$. For example, for a circle of radius $R = r$, $M(\theta) = r$, and one recovers the standard formulae: $L = 2\pi r$ and $A = \pi r^2$. When C is the convex hull of associated with the process at time t ,

we first need to compute its associated support function $M(\theta)$. A crucial point is to realize that actually $M(\theta) = \max_{0 \leq \tau \leq t} [x(\tau) \cos(\theta) + y(\tau) \sin(\theta)]$ [23, 24]. Furthermore, if the process is rotationally invariant any average is independent of the angle θ . Hence for the average perimeter we can simply set $\theta = 0$ and write $\langle L(t) \rangle = 2\pi \langle M(0) \rangle$, where brackets denote the ensemble average over realizations. Similarly for the average area, $\langle A(t) \rangle = \pi [\langle M^2(0) \rangle - \langle M'(0)^2 \rangle]$. Clearly, $M(0) = \max_{0 \leq \tau \leq t} [x(\tau)]$ is then the maximum of the one dimensional component process $x(\tau)$ for $\tau \in [0, t]$. Assuming that $x(\tau)$ takes its maximum value $x(t_m)$ at time $\tau = t_m$ (see Fig. 4). Then, $M(0) = x(t_m) = x_m(t)$, and $M'(0) = y(t_m)$ [31]. Now, by taking the average over Cauchy's formulas, and using isotropy, we simply have Eqs. [5] and [6] for the mean perimeter and the mean area of the convex hull C at time t . Note that this argument is very general and is applicable to any rotationally invariant two dimensional stochastic process. Since the branching Brownian motion with death is rotationally invariant we can use these formulae.

Numerical methods. Numerical integration. Equations [9] and [14] have been integrated numerically by finite differences in the following way. Time has been discretized by setting $t = ndt$, and space by setting $x = idx$, where dt and dx are small constants. For the sake of simplicity, here we consider the case $R_0 = 1$. We thus have

$$\begin{aligned} Q_{n+1}(i) &= \\ &= Q_n(i) + \gamma dt [1 - Q_n(i)]^2 + \\ D \frac{dt}{(dx)^2} [Q_n(i+1) - 2Q_n(i) + Q_n(i-1)] \end{aligned} \quad [23]$$

and

$$\begin{aligned} T_{n+1}(i) &= \\ &= T_n(i) + 2\gamma dt T_n(i) [Q_n(i) - 1] + \\ D \frac{dt}{(dx)^2} [T_n(i+1) - 2T_n(i) + T_n(i-1)] + \\ &\quad \frac{dt}{dx} [T_n(i) - T_n(i-1)]. \end{aligned} \quad [24]$$

As for the initial conditions, $Q_0(0) = 0$ and $Q_0(i > 0) = 1$, and $T_0(i) = 0 \forall i$. The boundary conditions at the origin are $Q_n(0) = 0$ and $T_n(0) = 0$. In order to implement the boundary condition at infinity, we impose $Q_n(i_{\max}) = 1$ and $T_n(i_{\max}) = 0 \forall n$, where the large value i_{\max} is chosen so that $T_n(i_{\max}) - T_n(i_{\max} - 1) < 10^{-7}$. We have verified that numerical results do not change when passing to the tighter condition $T_n(i_{\max}) - T_n(i_{\max} - 1) < 10^{-9}$.

Once $Q_n(i)$ and $T_n(i)$ are known, we use Eqs. [10] and [15] to determine the average perimeter and area, respectively.

Monte Carlo simulations. The results of numerical integrations have been confirmed by running extensive Monte Carlo simulations. Branching Brownian motion with death has been simulated by discretizing time with a small dt : in each interval dt , with probability bdt the walker branches and the current walker coordinates are copied to create a new initial point, which is then stored for being simulated in the next dt ; with probability γdt the walker dies and is removed; with probability $1 - (b + \gamma)dt$ the walker diffuses: the x and y displacements are sampled from Gaussian densities of zero mean and standard deviation $\sqrt{2Ddt}$ and the particle position is updated. The positions of all the random walkers are recorded as a function of time and the corresponding convex hull is then computed by resorting to the algorithm proposed in [32].

Perimeter statistics. In order to complete the analysis of the convex hull statistics, in Fig 6 and Fig 7 we show the results for the perimeter.

Analysis of t_m . In the critical case $R_0 = 1$, the stationary joint probability density $P_\infty(x_m, t_m)$ satisfies (upon setting $\partial P_t / \partial t = 0$ in Eq. [12])

$$\begin{aligned} \frac{\partial}{\partial t_m} P_\infty(x_m, t_m) &= \\ &= \left[D \frac{\partial^2}{\partial x_m^2} - \frac{2\gamma}{\left[1 + \sqrt{\frac{\gamma}{6D}} x_m\right]^2} \right] P_\infty(x_m, t_m). \end{aligned} \quad [25]$$

For any $x_m > 0$, we have the condition $P_\infty(x_m, 0) = 0$. The boundary conditions for Eq. (25) are $P_\infty(x_m \rightarrow \infty, t_m) = 0$ and $P_\infty(0, t_m) = q_\infty(0) \delta(t_m) = 2\sqrt{\gamma/(6D)} \delta(t_m)$. We first take the Laplace transform of (25), namely,

$$\tilde{P}_\infty(x_m, s) = \int_0^\infty e^{-st_m} P_\infty(x_m, t_m) dt_m. \quad [26]$$

This gives for all $x_m > 0$

$$\frac{D}{s} \frac{\partial^2}{\partial x_m^2} \tilde{P}_\infty(x_m, s) = \left[1 + \frac{12}{\frac{s}{D} \left(\sqrt{\frac{6D}{\gamma}} + x_m\right)^2} \right] \tilde{P}_\infty(x_m, s), \quad [27]$$

where we have used the condition $P_\infty(x_m, 0) = 0$ for any $x_m > 0$. This second order differential equation satisfies two boundary conditions: $\tilde{P}_\infty(\infty, s) = 0$ and $\tilde{P}_\infty(0, s) = 2\sqrt{\gamma/(6D)}$. The latter condition is obtained by Laplace transforming $P_\infty(0, t_m) = 2\sqrt{\gamma/(6D)} \delta(t_m)$. By setting

$$z = \left(\sqrt{\frac{6D}{\gamma}} + x_m \right) \sqrt{\frac{s}{D}}, \quad [28]$$

we rewrite the equation as

$$\frac{\partial^2}{\partial z^2} \tilde{P}_\infty - \tilde{P}_\infty - \frac{12}{z^2} \tilde{P}_\infty = 0. \quad [29]$$

Upon making the transformation $\tilde{P}_\infty(z) = \sqrt{z} F(z)$, the function $F(z)$ then satisfies the Bessel differential equation

$$\frac{d^2}{dz^2} F(z) + \frac{1}{z} \frac{d}{dz} F(z) - \left[1 + \frac{49}{4z^2} \right] F(z) = 0. \quad [30]$$

The general solution of this differential equation can be expressed as a linear combination of two independent solutions: $F(z) = A I_{7/2}(z) + B K_{7/2}(z)$ where $I_\nu(z)$ and $K_\nu(z)$ are modified Bessel functions. Since, $I_\nu(z) \sim e^z$ for large z , it is clear that to satisfy the boundary condition $\tilde{P}_\infty(\infty, s) = 0$ (which mean $F(z \rightarrow \infty) = 0$), we need to choose $A = 0$. Hence we are left with $F(z) = B K_{7/2}(z)$, where the constant B is determined from the second boundary condition

$\tilde{P}_\infty(0, s) = 2\sqrt{\gamma/(6D)}$. By reverting to the variable x_m , we finally get

$$\tilde{P}_\infty(x_m, s) = 2\sqrt{\frac{\gamma}{6D}} \sqrt{1 + \frac{\gamma}{6D} x_m} \frac{K_{7/2} \left[\left(\sqrt{\frac{6D}{\gamma}} + x_m \right) \sqrt{\frac{s}{D}} \right]}{K_{7/2} \left[\sqrt{\frac{6s}{\gamma}} \right]}. \quad [31]$$

Now, we are interested in determining the Laplace transform of the marginal density $\tilde{p}_\infty(s) = \int_0^\infty e^{-st_m} p_\infty(t_m) dt_m$ where $p_\infty(t_m) = \int_0^\infty P_\infty(x_m, t_m) dx_m$. Taking Laplace transform of this last relation with respect to t_m gives $\tilde{p}_\infty(s) = \int_0^\infty \tilde{P}_\infty(x_m, s) dx_m$. Once we know $\tilde{p}_\infty(s)$, we can invert it to obtain $p_\infty(t_m)$. Since we are interested only in the asymptotic tail of $p_\infty(t_m)$, it suffices to investigate the small s behavior of $\tilde{p}_\infty(s)$. Integrating Eq. (31) over x_m and taking the $s \rightarrow 0$ limit, we obtain after some straightforward algebra

$$\tilde{p}_\infty(s) = 1 + \frac{3}{5\gamma} s \ln(s) + \dots \quad [32]$$

We further note that

$$\int_0^\infty e^{-st_m} t_m^2 p_\infty(t_m) dt_m = \frac{d^2}{ds^2} \tilde{p}_\infty(s) \simeq \frac{3}{5\gamma s}, \quad [33]$$

which can then be inverted to give the following asymptotic behavior for large t_m

$$p_\infty(t_m) \simeq \frac{3}{5\gamma t_m^2}. \quad [34]$$

Analogously as for $\langle x_m^2 \rangle$, the moment $\langle t_m \rangle \rightarrow \infty$, due to the power-law tail $p_\infty(t_m) \propto t_m^{-2}$. Hence we need to compute $\langle t_m \rangle$ for large but finite t : in this case, the time-dependent solution displays a scaling behavior

$$p_t(t_m) \simeq p_\infty(t_m) g\left(\frac{t_m}{t}\right), \quad [35]$$

where the scaling function $g(z)$ satisfies the conditions $g(z \ll 1) \simeq 1$ and $g(z \gg 1) = 0$. Much like in Eq. [17] for the marginal density $q_t(x_m)$, we have a power-law tail of $p_t(t_m)$ for large t_m that has a cut-off at a scale $t_m^* \sim t$, and $g(z)$ is the cut-off function. As in the case of x_m , we do not need the precise form of $g(z)$ to compute the leading term of the first moment $\langle t_m \rangle = \int_0^\infty p_t(t_m) t_m dt_m$ for large t . Cutting off the integral at $t_m^* = c_1 t$ (where c_1 depends on the precise form of $g(z)$) and performing the integration gives

$$\langle t_m \rangle \simeq \int_0^t t_m p_\infty(t_m) dt_m \simeq \frac{3}{5\gamma} \ln t, \quad [36]$$

which is precisely the result announced in Eq. [19].

ACKNOWLEDGMENTS.

S.N.M. acknowledges support from the ANR grant 2011-BS04-013-01 WALK-MAT. S.N.M and A.R. acknowledge support from the Indo-French Centre for the Promotion of Advanced Research under Project 4604-3.

1. Bailey N T J (1975) *The Mathematical Theory of Infectious Diseases and its Applications*, Griffin, London
2. McKendrick A G (1925) Applications of mathematics to medical problems. *Kapil Proceedings of the Edinburgh Mathematical Society* 44:1-34
3. P. Whittle (1955) The outcome of a stochastic epidemic - a note on Baileys paper. *Biometrika* 42:116122
4. Murray J D (1989) *Mathematical Biology*, Springer-Verlag, Berlin
5. Bartlett M S (1960) *Stochastic Population Models in Ecology and Epidemiology*
6. Andersson H, Britton T (2000) *Stochastic Epidemic Models and their Statistical Analysis Lecture Notes in Statistics 151*, Springer-Verlag, New York
7. Antal T, Kravivsky P L (2012) Outbreak size distributions in epidemics with multiple stages. arXiv:1204.4214
8. Anderson R, May R (1991) *Infectious Diseases: Dynamics and Control*, Oxford University Press, Oxford
9. Antia R, Regoes R R, Koella J C, Bergstrom C T (2003) The role of evolution in the emergence of infectious diseases. *Nature* 426:658-661

10. Kendall D G (1956) Deterministic and stochastic epidemics in closed populations. In Proc. 3rd Berkeley Symp. Math. Statist. Prob. 4:149-165
11. Bartlett M S (1956) An introduction to stochastic processes, Cambridge University Press
12. Elliott P, Wakefield J C, Best N G, Briggs D J (2000) Spatial Epidemiology: Methods and Applications, Oxford University Press
13. Radcliffe J (1976) The Convergence of a Position-Dependent Branching Process Used as an Approximation to a Model Describing the Spread of an Epidemic. Journal of Applied Probability 13:338-344
14. Wang J S (1980) The Convergence of a Branching Brownian Motion Used as a Model Describing the Spread of an Epidemic. Journal of Applied Probability 17:301-312
15. Riley S, et al (2007) Large-Scale Spatial-Transmission Models of Infectious Disease. Science 316:1298-1301
16. Fraser C, et al (2009) Pandemic Potential of a Strain of Influenza A (H1N1): Early Findings Science 324:1557-1561
17. Colizza V, Barrat A, Barthélemy M, Vespignani A (2006) The role of the airline transportation network in the prediction and predictability of global epidemics. Proc. Natl. Acad. Sci. USA 103:2015
18. Brockmann D, Hufnagel L, Geisel T (2006) The scaling laws of human travel. Nature 439:462-465
19. Cowled B, Ward M P, Hamilton S, Garner G (2009) The equine influenza epidemic in Australia: Spatial and temporal descriptive analyses of a large propagating epidemic. Preventive Veterinary Medicine 92:6070
20. Worton B J (1995) A convex hull-based estimator of home-range size. Biometrics 51: 1206-1215
21. Giuggioli L, Abramson G, Kenkre V M, Parmenter R R, Yates T L (2006) Theory of home range estimation from displacement measurements of animal populations. J. Theor. Biol. 240: 126-135.
22. Sawyer S and Fleischman J (1979) Maximum geographic range of a mutant allele considered as a subtype of a Brownian branching random field. Proc Natl Acad Sci USA 76:872875.
23. Randon-Furling J, Majumdar S N, Comtet A (2009) Convex Hull of N planar Brownian Motions: Application to Ecology. Phys. Rev. Lett. 103:140602
24. Majumdar S N, Comtet A, Randon-Furling J (2010) Random Convex Hulls and Extreme Value Statistics. J. Stat. Phys. 138:955-1009
25. Reymbaut A, Majumdar S N, Rosso A (2011) The Convex Hull for a Random Acceleration Process in Two Dimensions. J. Phys. A-Math. & Theor. 44:415001
26. Cauchy A (1850) Mem. Acad. Sci. Inst. Fr. 22: 3 ; see also the book by L. A. Santaló, Integral Geometry and Geometric Probability (Addison-Wesley, Reading, MA, 1976)
27. van Saarloos W (2003) Front propagation into unstable states. Phys. Rep. 386: 29-222.
28. Brunet E, Derrida B (2009) Statistics at the tip of a branching random walk and the delay of traveling waves Europhys. Lett. 87:60010.
29. Majumdar S N, Krapivsky P L (2003) Extreme value statistics and traveling fronts: various applications. Physica A 318:161-170.
30. A. Cauchy (1850), Mem. Acad. Sci. Inst. Fr. 22, 3; see also the book by L. A. Santaló, Integral Geometry and Geometric Probability (Addison-Wesley, Reading, MA, 1976).
31. Actually, t_m implicitly depends on θ , hence formally $M'(\theta) = -x(t_m) \sin(\theta) + y(t_m) \cos(\theta) + \frac{dt_m}{d\theta} \frac{dz_\theta(t)}{dt} \Big|_{t=t_m}$. Nonetheless, since $z_\theta(t)$ is maximum at $t = t_m$, by definition $dz_\theta(t)/dt|_{t=t_m} = 0$.
32. Module: Finding the convex hull of a set of 2D points, by Gehrman D C, Python Cookbook, edited by Martelli A and Ascher D

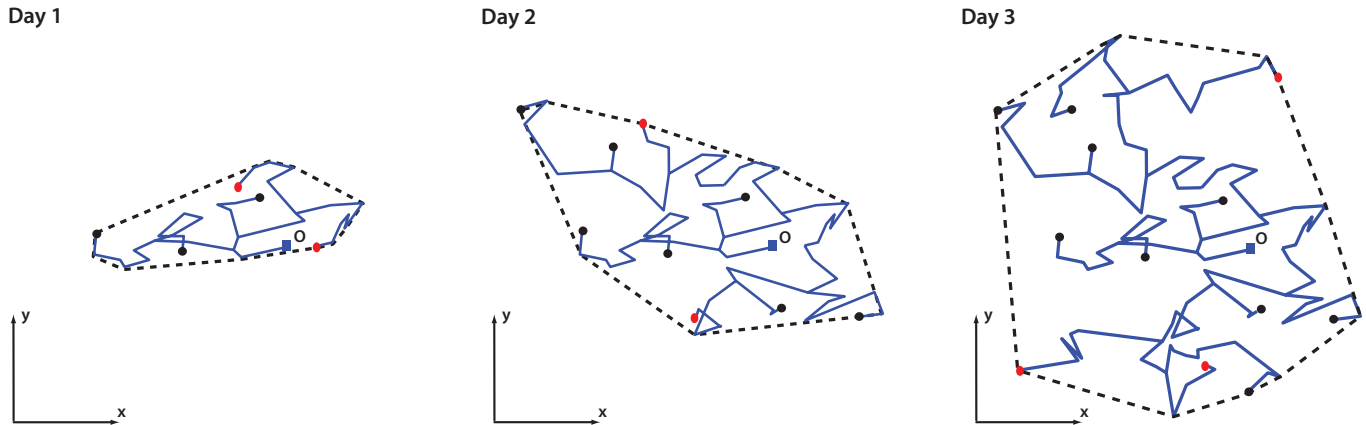


Fig. 1. The snapshots of the trajectories of an assembly of infected individuals at the epidemics outbreak at three different times (schematic), starting from a single infected at the origin O at time $t = 0$. Individuals that are still infected at a given time t are displayed as red dots, while those already recovered are shown as black dots. The convex hull enclosing the trajectories (shown as a dashed line) is a measure of geographical area covered by the spreading epidemic. As the epidemic grows in space, the associated convex hull also grows in time.

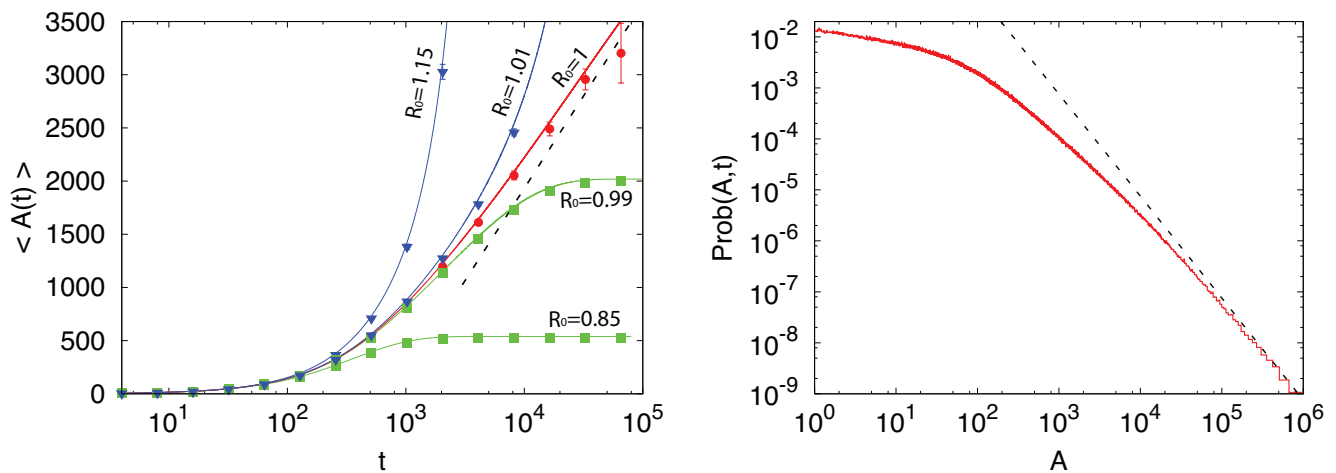


Fig. 2. Left. The average area $\langle A(t) \rangle$ of the convex hull as a function of the observation time. For the parameter values, we have chosen $D = 1/2$ and $b = R_0\gamma = 0.01$. We considered five different values of R_0 . We have obtained these results by two different methods: (i) via the numerical integration of Eqs. [9] and [14] and using Eq. [15]. These results are displayed as solid lines. (ii) by Monte Carlo simulations of the two-dimensional branching Brownian motion with death with the same parameters, averaged over 10^5 samples. Monte Carlo are displayed as symbols. The dashed lines represent the asymptotic limits as given in Eq. [2] for the critical case $R_0 = 1$. Further details of the numerical simulations are provided in the Supplementary Material. Right. Distribution of the area of the convex hull for the critical case $R_0 = 1$, with $\gamma = 0.01$ and $D = 1/2$, as obtained by Monte Carlo simulations with $2 \cdot 10^6$ realizations. The dashed line corresponds to the power-law $(24\pi D/5\gamma)A^{-2}$ as predicted by Eq [20].

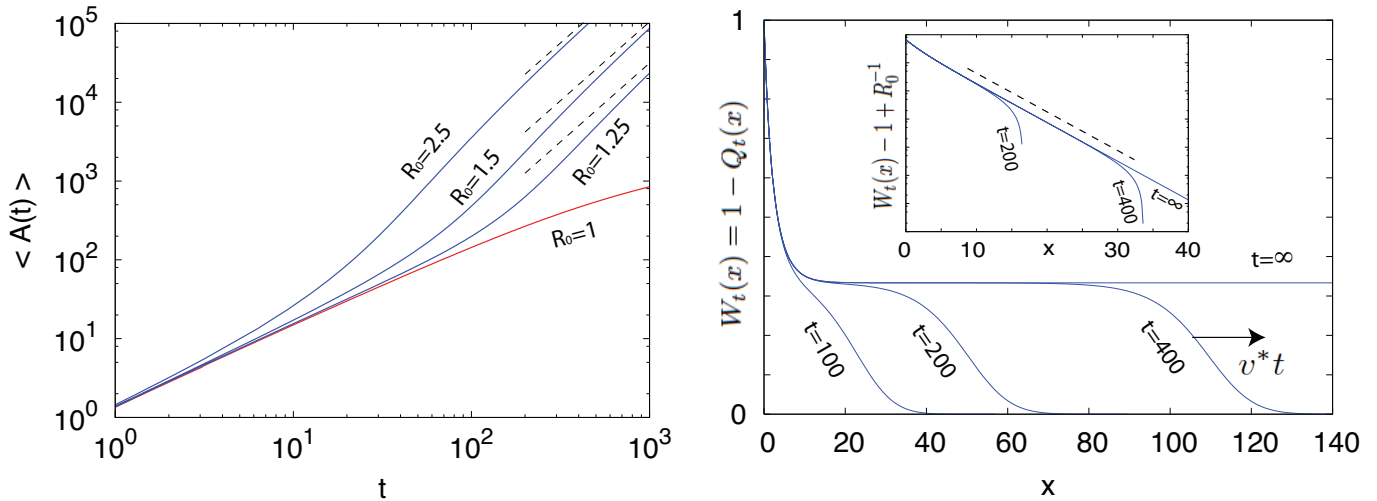


Fig. 3. Left. The time behavior of the average area in the supercritical regime for different values of $R_0 > 1$. Dashed lines represent the asymptotic scaling as in Eq. [4]. The red curve corresponds to the critical regime. Right. The behavior of $W_t(x) = 1 - Q_t(x)$ for $R_0 = 1.5$ at different times, as in Eq. [21]. When $t \rightarrow \infty$, $W_t(x) \rightarrow 1 - R_0^{-1}$, and for large but finite times the travelling front behavior is clearly visible. The inset displays the exponential convergence of $W_t(x)$ to the asymptotic limit. The dashed line represents $\xi = \sqrt{D/\gamma(R_0 - 1)}$.

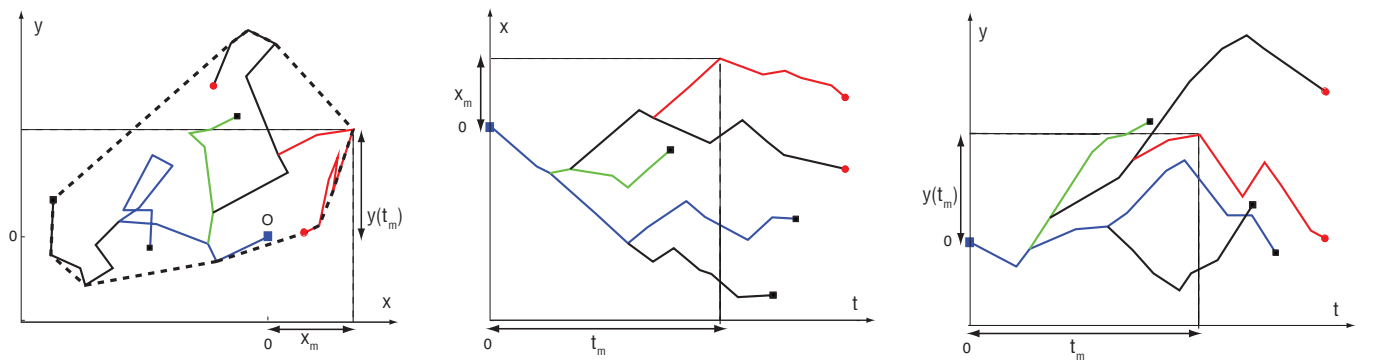


Fig. 4. Left. A branching random walk composed of five individuals. At time $t = 0$, a single infected is at the origin O , and starts diffusing (blue line). At later times, this individual branches and gives rise to other infected individuals. Among these, the red path reaches the maximum x_m along the x component up to the final time t . Infected individuals at a given time t are displayed as red dots, whereas recovered as black dots. Center. The displacement along the x direction as a function of time. The red path reaches the global maximum x_m at time t_m . Right. The displacement along the y direction as a function of time. When the red path reaches the global maximum x_m at time t_m , its y coordinate attains the value $y(t_m)$. A crucial observation is that the y component of the trajectory connecting O to the red path is a regular Brownian motion. This is not the case for the x component, which is constrained to reach the global maximum of the branching process.

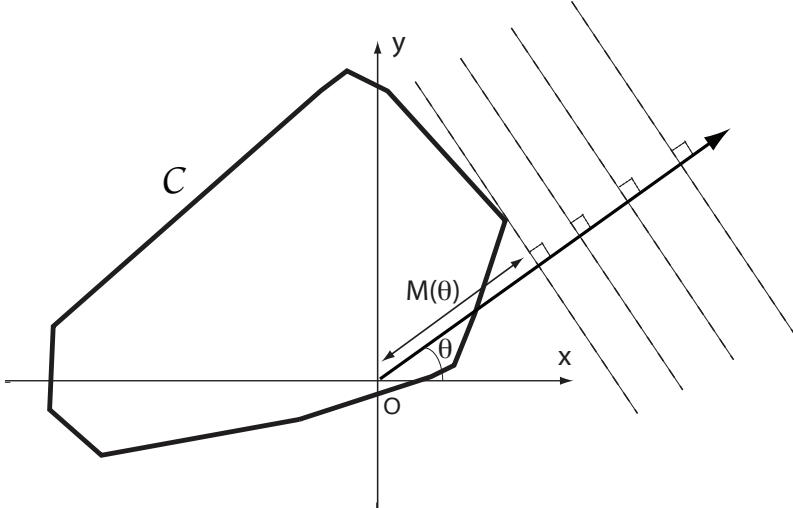


Fig. 5. Cauchy's construction of the two-dimensional convex hull, with support function $M(\theta)$ representing the distance along the direction θ .

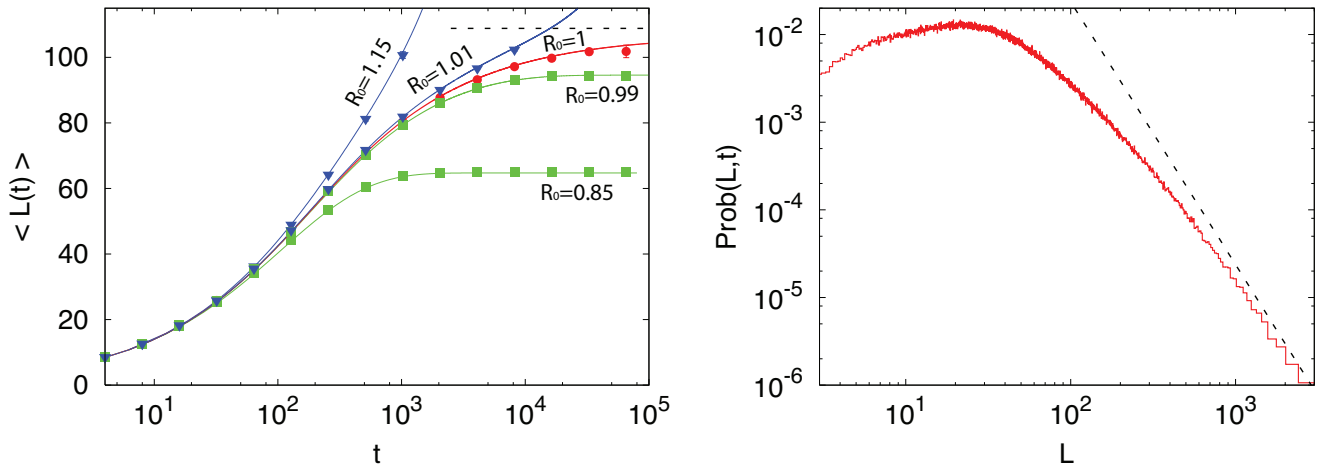


Fig. 6. Left. The average perimeter $\langle L(t) \rangle$ of the convex hull as a function of the observation time. For the parameter values, we have chosen $D = 1/2$ and $b = R_0 \gamma = 0.01$. We considered five different values of R_0 . We have obtained these results by two different methods: (i) via the numerical integration of Eq. [9] and using Eq. [10] (with the choices $dt = 0.003125$ and $dx = 0.1768$). These results are displayed as solid lines. (ii) by Monte Carlo simulations of the two-dimensional branching Brownian motion with death with the same parameters and with the choice of the Monte Carlo time step $dt = 0.25$ with the results averaged over 10^5 samples. Monte Carlo are displayed as symbols. The dashed lines represent the asymptotic limits as given in Eq. [1] for the critical case $R_0 = 1$. Right. Distribution of the perimeter of the convex hull for the critical case $R_0 = 1$, with $\gamma = 0.01$ and $D = 1/2$, as obtained by Monte Carlo simulations with time step $dt = 1$ and $t = 4 \cdot 10^5$. The number of realizations is $2 \cdot 10^6$. The dashed line of the left panel corresponds to the power-law L^{-3} (up to an arbitrary prefactor).

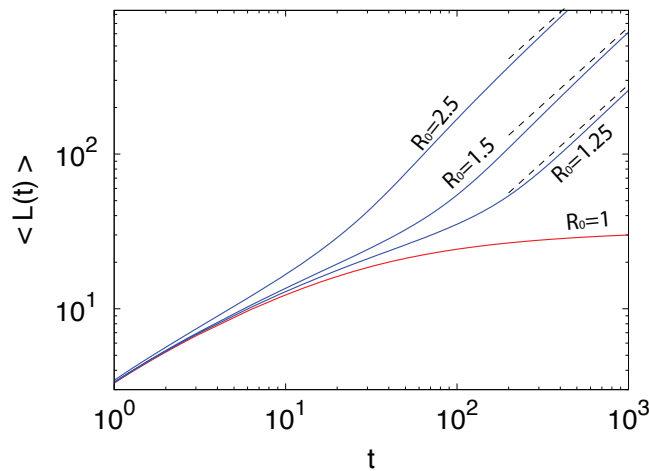


Fig. 7. The time behavior of the average perimeter in the supercritical regime for different values of $R_0 > 1$. Dashed lines represent the asymptotic scaling as in Eq. [3]. The red curve corresponds to the critical regime.